RSC Advances

PAPER

View Article Online
View Journal | View Issue

Cite this: *RSC Adv.*, 2025, **15**, 39871

Preparation of thiol-functionalized polyurethane foam and its adsorption performance for Hg(II)

Meixin Chen,[a] Lili Zhu, [a] Juan Jin,[a] Cunxin Sun[a] and Zhenjiang Zhang *[b]

Received 25th July 2025
Accepted 13th October 2025

DOI: 10.1039/d5ra05379j

rsc.li/rsc-advances

To address the challenges of heavy metal mercury-induced water pollution and the recycling difficulties of polyurethane foam, this study modified waste polyurethane foam (PUF) using γ-mercaptopropyl trimethoxysilane (NQ590) to prepare thiol-functionalized polyurethane foam (PUF-HS). The adsorption mechanism of PUF-HS toward Hg(II) was investigated *via* adsorption kinetics and isothermal adsorption models. Results showed that the modified foam surface displayed protruding particles formed by silane condensation, while the matrix foam maintained its highly porous three-dimensional network structure. The adsorption equilibrium time of PUF-HS for Hg(II) was determined to be 510 min. Kinetics and isothermal analyses revealed that the adsorption process conformed well to the pseudo-second-order kinetics model and the Freundlich isotherm model, respectively. The adsorption was multilayer adsorption dominated by chemical adsorption and controlled by intra-particle diffusion and film diffusion. According to Langmuir isotherm model fitting, the maximum adsorption capacity of PUF-HS for Hg(II) at 35 °C was 35.96 mg g^{-1}. This study enabled the resource utilization of waste polyurethane foam and developed a novel adsorbent material for efficient removal of toxic heavy metal ion Hg(II) from water.

1. Introduction

With the rapid development of modern chemical industry, various pollution problems have arisen. Industries such as mining, smelting, textiles, dyeing, and metal processing emit large amounts of heavy metal pollutants such as As, Pb, Hg, and Cr,[1] posing significant threats to the environment.[2] Toxic heavy metals in wastewater may alter their chemical composition when mixed with soil and water bodies in natural ecosystems,[3] thereby expanding the scope of pollution. Among these pollutants, Hg stands out as a primary environmental hazard, characterized by its neurotoxicity and damage to vital organs (*e.g.*, liver and kidneys).[4] Acute and chronic Hg exposure has long been recognized as a critical public health concern.[5] Although the World Health Organization (WHO) has set an occupational exposure limit of 0.005 mg m^{-3} for Hg vapor in the workplace,[6] persistent environmental contamination indicates the challenge of completely eliminating Hg. Effective technical measures are thus required to convert it into less toxic forms, thereby mitigating its impact on human health.[7]

To address the issue of Hg(II) pollution in water, researchers have employed diverse methods for treating Hg(II)-contaminated wastewater, including adsorption, solvent extraction, coagulation, microfiltration, and oxidation.[8] Among these, adsorption has emerged as the most effective approach due to its operational simplicity, cost-efficiency, reusability, and high regenerability.[9] Adsorption refers to the enrichment of solutes on the surface or interfacial region of an adsorbent.[10] Functionalization of adsorbents can effectively regulate their selectivity and adsorption capacity. Most functional adsorbents are prepared *via* traditional chemical methods or by modifying natural adsorbent materials with inherently low adsorption capacity. Therefore, the development of inexpensive, efficient, environmentally friendly, and energy-efficient adsorbents has remained a consistent objective in the advancement of adsorption technology.

Polyurethane foam (PUF) finds extensive practical applications in fields such as building decoration, medical equipment, and thermal insulation.[11] It boasts advantages including high porosity, low cost, large specific surface area, facile chemical functionalization, and easy separation from aqueous solutions. Modified polyurethane-based adsorbents also serve as superior polymer adsorbents for wastewater treatment.[12] By introducing various multifunctional groups onto PUF, its specific surface area, selectivity, and interactions *via* hydrogen bonding and ionic bonding can be enhanced, thereby improving its pollutant adsorption capacity.[13,14] However, the preparation processes in the previous studies are mostly complex and energy-intensive, which does not align with the principles of green and environmental sustainability. In addition, PUF is notoriously difficult to recycle, and discarded PUF poses significant challenges for

---

[a] *School of Chemistry and Chemical Engineering, Ludong University, Yantai 264025, China*

[b] *School of Materials Science and Engineering, Ludong University, Yantai 264025, China. E-mail: zhangzhj365@126.com*

environmental management and waste disposal. This study reports the modification of discarded PUF using γ-mercaptopropyl trimethoxysilane to prepare a novel thiol-functionalized polyurethane foam (PUF-HS). PUF-HS contains imine and thiol groups, which serve as direct binding sites for Hg(II), potentially enhancing PUF's adsorption capacity for Hg(II) and enabling its application in removing toxic heavy metal Hg(II) from wastewater. The PUF used in this work was derived from discarded foam, offering an advantage over traditional methods by avoiding additional waste generation and enabling cost-effective extraction of toxic heavy metal ions. The preparation of PUF-HS involved a two-step process: first, PUF was roughened using a mixture of H_2SO_4 and CrO_3 solutions, and then the roughened foam was used as a carrier to graft γ-mercaptopropyl trimethoxysilane in an ethanol solution, yielding PUF-HS. Various characterization techniques were employed to analyze the morphological structure of PUF-HS. PUF-HS was evaluated as an adsorbent for Hg(II) removal, with its adsorption performance and mechanism systematically investigated. This study provides a new approach to solving the problems of reusing waste PUF and removing Hg(II) pollution from the aquatic environment.

2. Experimental section

2.1. Chemicals and materials

Discarded polyurethane foam (scrap from sofa factories), chromium trioxide, γ-mercapto propyl trimethoxysilane, anhydrous ethanol, concentrated sulphuric acid, concentrated hydrochloric acid, sodium hydroxide, mercury chloride, lead nitrate, copper nitrate, nickel nitrate, zinc nitrate, sodium chloride and humic acid were purchased from Sinopharm Chemical Reagents Co., Ltd.

2.2 Characterization methods

The surface morphology of waste PUF, roughened PUF, and PUF-HS was studied using a field emission scanning electron microscope (SEM, SU8010, Hitachi, Japan) at 15 kV. The types and contents of elements in the adsorbent were analyzed using an energy dispersive spectrometer (EDS, X-Flash/6160, Bruker, Germany). The specific surface area, pore volume, and pore size distribution of the adsorbent were characterized using a surface area and porosity analyzer (BET method; ASAP 2460, Micromeritics, USA).

The infrared absorption spectra of the adsorbent were measured using a Fourier transform infrared spectrometer (FTIR, Nicolet iS50, Thermo Scientific, USA), and the functional groups of PUF-HS were analyzed. The elemental composition and valence states of the samples were analyzed using an X-ray photoelectron spectrometer (XPS, ESCALAB XI+, Thermo Scientific, USA). The thermal stability of PUF-HS was determined using a thermogravimetric analyzer (TGA, TGA2, METTLER TOLEDO, Switzerland) under a nitrogen atmosphere, with a testing temperature range of 30–600 °C and a heating rate of 10 °C min^{-1}.

2.3 Synthesis of PUF-HS

2.3.1 Pre-treatment of PUF. The PUF was pre-treated by first being cut into 2 cm × 2 cm cube-like pieces, followed by ultrasonic cleaning in a 20 wt% ethanol solution for 1 h. It was then ultrasonically cleaned in pure water for 1 h, dried at 60 °C for 3 h, immersed in a roughening solution (100 g L^{-1} concentrated H_2SO_4 and 200 g L^{-1} CrO_3) for 60 seconds, rinsed 12 times with pure water, dried at 60 °C for 3 h, and finally dried at room temperature for 12 h to obtain the roughened PUF,[15] labelled as pre-PUF. The synthesis of pre-PUF was illustrated in Fig. 1.

2.3.2 Preparation of thiol-modified PUF. The preparation of thiol-modified PUF is as follows: a 20 wt% ethanol solution was prepared, and its pH was adjusted to 3.6 using 0.1 mol L^{-1} hydrochloric acid. An appropriate amount of γ-mercaptopropyl trimethoxysilane (NQ590) was added to 60 mL of the ethanol solution, followed by sonication for 13 min to yield a white homogeneous mixture. Pre-PUF (0.5 g) was then added to the mixture, which was stirred under reflux at 40 °C in a water bath for 2 h. The foam was subsequently removed, filtered under reduced pressure for 10 min, alternately washed three times with anhydrous ethanol and pure water, and vacuum-dried at 60 °C for 3 h to obtain the thiol-modified PUF, denoted as PUF-HS. The synthesis of PUF-HS was illustrated in Fig. 1.

2.4 Study on the adsorption performance of PUF-HS for Hg(II)

The adsorption performance of PUF-HS toward Hg(II) in aqueous solutions was investigated *via* the static batch adsorption method. Batch adsorption experiments were performed in 100 mL stoppered conical flasks, which were shaken in a thermostatic shaker (SHY-2A) at 180 rpm.

Investigating the effect of solution pH on the adsorption of Hg(II) by PUF-HS is a crucial step in heavy metal adsorption research. Generally, Hg(II) exists as free ions when solution pH < 3.2; as $Hg(OH)^+$ species at pH 4–6; precipitates as hydroxides at pH 7–10; and converts to $Hg(OH)_3^-$ anions when pH > 10.[16] Therefore, the adsorption performance of PUF-HS toward Hg(II) was investigated at pH 1.0–6.0. The initial pH of the Hg(II) solution was adjusted using 1 mol L^{-1} HCl and 0.1 mol L^{-1} NaOH. The adsorbent mass was 50 mg, the solution volume was 20 mL, and the initial concentration was 100.0 mg L^{-1}.

The effect of adsorption time on Hg(II) adsorption by PUF-HS was investigated as follows: 50 mg of PUF-HS was added to 20 mL of Hg(II) solution (100.0 mg L^{-1}, pH 6.0) at 25 °C. Samples were withdrawn at different time points (10, 20, 30, 40, 80, 100, 120, 160, 200, 240, 300, 360, 420, 510, and 600 min), and the residual Hg(II) concentration in the supernatant was measured.

The effect of different initial Hg(II) concentrations on its adsorption by PUF-HS was investigated. Specifically, 50 mg of PUF-HS was immersed in 20 mL of solutions with pH 6.0 and varying concentrations (29.9, 49.4, 79.0, 99.1, 154.1, 181.3, 211.6 mg L^{-1}). The mixtures were shaken in a thermostatic shaker for 12 h.

The adsorption selectivity of PUF-HS toward Hg(II) was investigated by evaluating its adsorption performance in

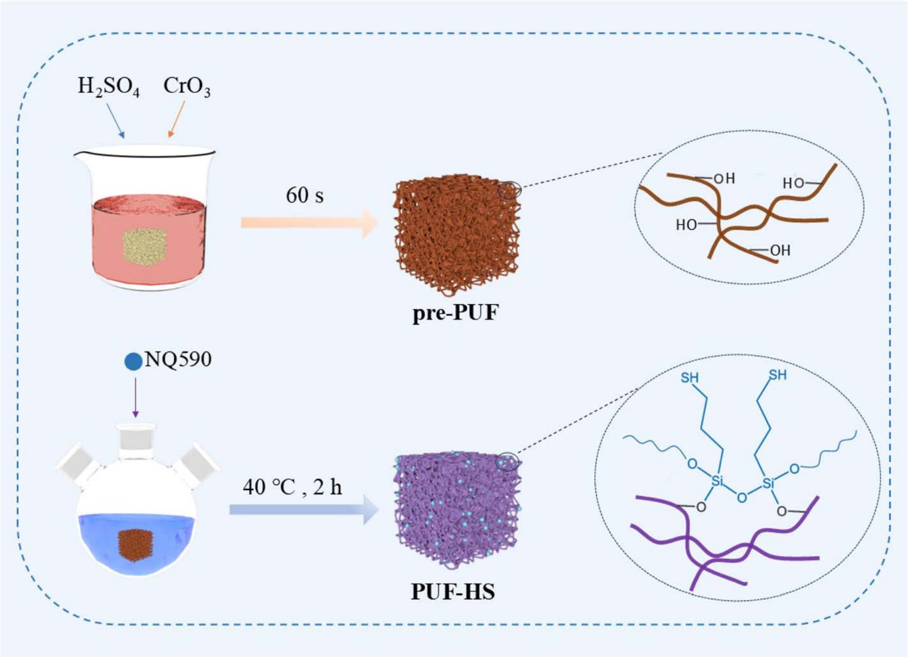

Fig. 1 Synthesis of pre-PUF and PUF-HS.

solutions containing single and mixed heavy metal ions (Hg(II), Pb(II), Cu(II), Zn(II), Ni(II)).

To investigate the effect of ionic strength on Hg(II) adsorption by PUF-HS, the adsorption performance of PUF-HS toward Hg(II) was evaluated in NaCl solutions with concentrations ranging from 0.01 to 0.1 mol L^{-1}. Similarly, to assess the influence of natural organic matter on Hg(II) adsorption by PUF-HS, the adsorption performance of PUF-HS toward Hg(II) was examined in humic acid solutions with concentrations of 20–40 mg L^{-1}.

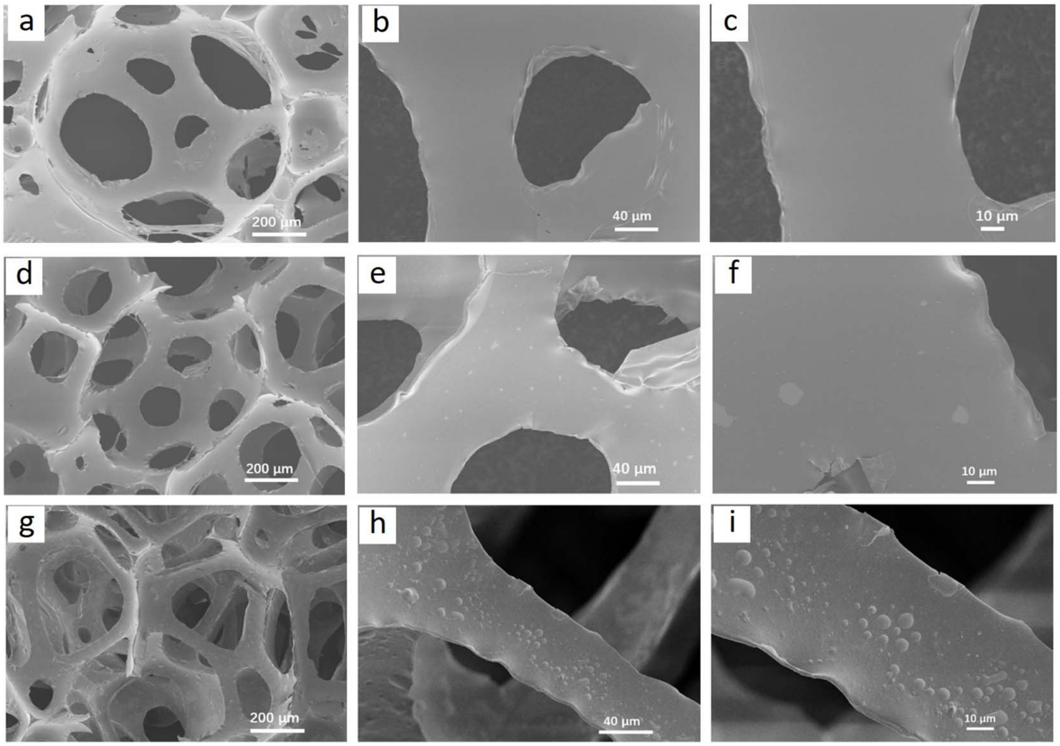

Fig. 2 SEM images of (a–c) PUF, (d–f) pre-PUF, and (g–i) PUF-HS.

The residual concentrations of Hg(II), Pb(II), Cu(II), Zn(II), and Ni(II) in the supernatant were determined by atomic absorption spectrophotometry (AAS, AA240, VARIAN, USA). All adsorption experiments were conducted in triplicate, and the mean values were reported. The adsorption capacity of PUF-HS for Hg(II) (q_t, mg g^{-1}) was calculated using eqn (1).

$$q_t = \frac{(c_0 - c_t)V}{m} \tag{1}$$

where c_0 and c_t denote the concentrations of the Hg(II) solution before and after adsorption (mg L^{-1}), respectively; q_t represents the adsorption amount at the adsorption time t (mg g^{-1}); V is the volume of the Hg(II) solution (L); and m is the mass of the adsorbent (g).

3 Results and discussion

3.1 Characterization of PUF, pre-PUF and PUF-HS

3.1.1 SEM-EDS and BET. The pore morphology and surface topography of PUF, pre-PUF, and PUF-HS were characterized using SEM. The pore walls of PUF were observed to be smooth, with a highly ordered three-dimensional porous network structure (Fig. 2a–c). After PUF coarsening treatment, the pre-PUF pore walls are etched, and the surface becomes rough (Fig. 2d–f). For PUF-HS (Fig. 2g–i), aggregated protruding particles appear on the surface of the bubble walls, which may be due to the grafting reaction and the self-condensation reaction of NQ590. As can be seen from the figure, PUF-HS still maintains a highly porous three-dimensional network structure. The foam skeleton was not damaged during the coarsening and grafting processes; only the surface became rougher compared to the original PUF.

The chemical composition of PUF-HS was characterized through EDS elemental spectrum. EDS results (Fig. 3) shows that PUF-HS consists of five elements: C, O, N, Si, and S, with relative contents of 61.79%, 26.07%, 10.68%, 0.79%, and 0.67%, respectively. SEM and EDS elemental spectrum results indicate that the PUF has been successfully modified with thiol modification.

BET analysis was performed on PUF-HS to determine its pore structure. The results shows that PUF-HS contained only microporous structure and no mesoporous. The BET-specific surface area and micropore volume of PUF-HS were 0.1428 m^2 g^{-1} and 0.000103 cm^3 g^{-1} respectively. And the average micropore size was 21.712 Å. For detailed results, please refer to the SI.

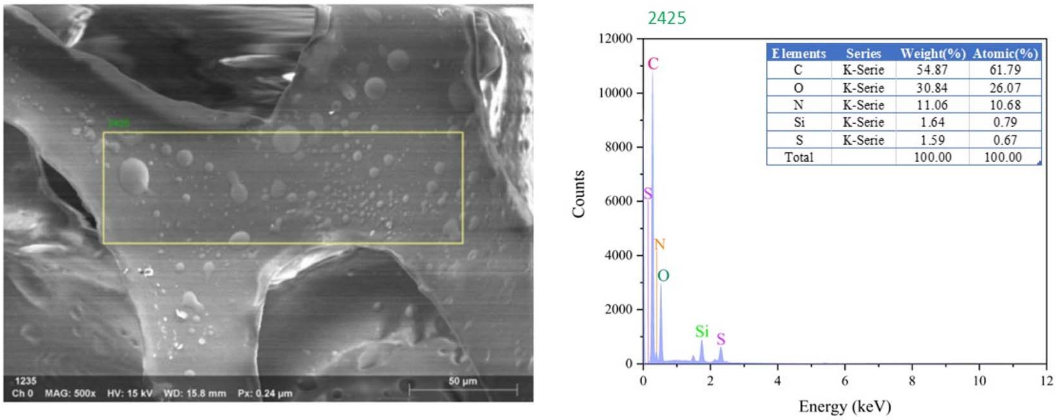

Elements	Series	Weight(%)	Atomic(%)
C	K-Serie	54.87	61.79
O	K-Serie	30.84	26.07
N	K-Serie	11.06	10.68
Si	K-Serie	1.64	0.79
S	K-Serie	1.59	0.67
Total		100.00	100.00

Fig. 3 EDS elemental spectrum of PUF-HS.

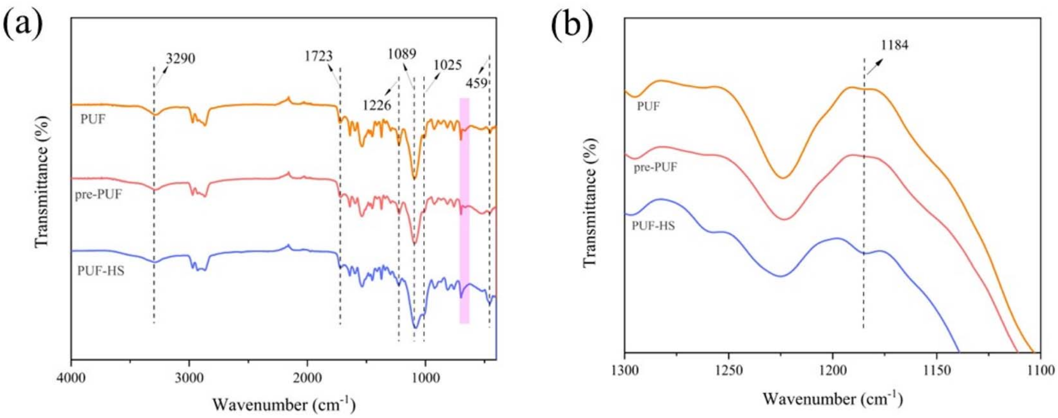

Fig. 4 FTIR analysis of PUF, pre-PUF and PUF-HS.

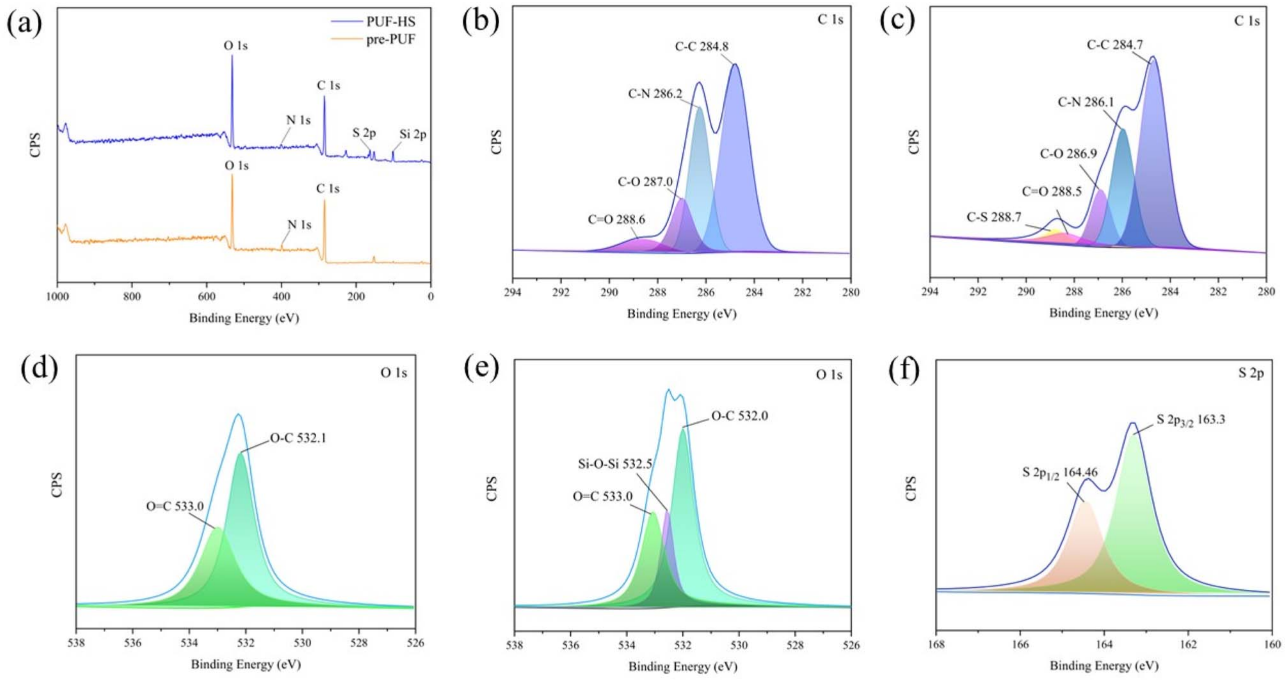

Fig. 5 (a) XPS full spectra of PUF-HS and pre-PUF; (b and c) high-resolution C 1s spectra of pre-PUF and PUF-HS; (d and e) high-resolution O 1s spectra of pre-PUF and PUF-HS; (f) high-resolution S 2p spectra of PUF-HS.

3.1.2 FTIR analysis. For the study of the structures and functional group information of PUF, pre-PUF, and PUF-HS, FTIR analysis was conducted in the range of 400–4000 cm^{-1}. As shown in Fig. 4a, characteristic absorption peaks of PUF at 3290, 1723, 1226, and 1089 cm^{-1} are attributed to the stretching vibrations of N–H, C═O, C–N, and C–O–C groups, respectively.[17] After roughening, the foam surface is oxidized to produce O–H, whose infrared peaks overlap with those of N–H. Therefore, the infrared peak near 3290 cm^{-1} corresponds to the stretching vibration peaks of both N–H and O–H groups. By normalizing to the C–O–C reference peak at 1089 cm^{-1}, the area ratios (A_{3290}/A_{1089}) for PUF and pre-PUF are quantified as 0.35 and 0.61, respectively, confirming the generation of O–H groups during the roughening process. For PUF-HS, the absorption feature at 459 cm^{-1} is attributed to the bending vibration of Si–O–Si groups.[18] Due to the stretching vibration of the Si–O–Si groups, the shoulder peak at 1025 cm^{-1} is strengthened.[19] The newly observed weak absorption peak at 1184 cm^{-1} corresponds to the C–S groups (Fig. 4b),[20] and the spectral modifications (peak shifts and intensity variations) in the 620–708 cm^{-1} region are ascribed to C–S stretching vibrations.[21] This indicates that γ-mercapto propyl trimethoxysilane has been successfully grafted onto PUF.

3.1.3 XPS analysis. XPS is usually used to analyze surface chemical composition and investigate the chemical state of elements. XPS was further used to characterize the structure of pre-PUF and PUF-HS foams, with the results shown in Fig. 5. In the full XPS spectra of pre-PUF and PUF-HS (Fig. 5a), three

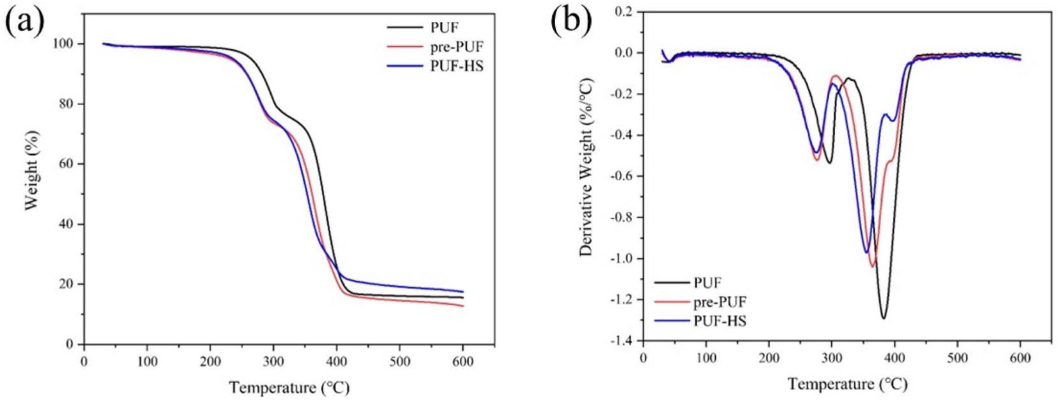

Fig. 6 (a) TG profiles of PUF, pre-PUF, and PUF-HS, (b) DTG profiles of PUF, pre-PUF, and PUF-HS.

peaks at 284.3, 399.5, and 532 eV are observed, corresponding to C 1s, N 1s, and O 1s, respectively. After thiol functionalization of pre-PUF, characteristic peaks of S and Si are observed in the full XPS spectra of PUF-HS.[22] The structures of pre-PUF and PUF-HS are further confirmed by high-resolution XPS spectra of C, O, and S. As shown in Fig. 5b, the characteristic peaks at 284.8, 286.2, 287.0, and 288.6 eV in the C 1s high-resolution spectrum of pre-PUF are attributed to C–C, C–N, C–O, and C═O, respectively. In the high-resolution C 1s spectrum of PUF-HS (Fig. 5c), a new characteristic peak at 288.7 eV appears is attributed to C–S.[22] As shown in Fig. 5d, the characteristic peaks at 532.1 and 533.0 eV in the O 1s high-resolution spectrum of pre-PUF are attributed to O–C and O═C, respectively. As shown in Fig. 5e, a new characteristic peak at 532.5 eV appears in the O 1s high-resolution spectrum of PUF-HS, which is attributed to Si–O–Si. In Fig. 5f, the S 2p peak of PUF-HS is split into two independent peaks, $2p_{3/2}$ and $2p_{1/2}$, due to spin–orbit energy level splitting, with peak positions at 163.3 and 164.5 eV, respectively, indicating the presence of –SH.[23,24] Therefore, the XPS results indicate that γ-mercapto-propyl trimethoxysilane is successfully grafted onto PUF, and thiol-modified polyurethane foam is successfully synthesized by the aforementioned method.

3.1.4 TG analysis. TG analysis was performed on PUF, pre-PUF, and PUF-HS under a N_2 protective atmosphere, with a test temperature range of 300–600 °C. Fig. 6a and b show the TG curves and differential thermal gravimetric (DTG) curves for PUF, pre-PUF, and PUF-HS, respectively. PUF has a multi-phase structure composed of hard segments and soft segments. The hard segments of PUF are more prone to thermal degradation and begin to degrade at lower temperatures.[25] As shown in Fig. 6a, PUF, pre-PUF, and PUF-HS all exhibit good thermal stability. PUF undergoes thermal degradation in two main stages. The first stage occurs between 258 °C and 308 °C, with a mass loss of approximately 17.58%. This stage of thermal degradation is associated with the degradation of the PUF hard segments, during which three reactions may occur simultaneously: the decomposition of isocyanates and alcohols, the formation of primary amines and olefins, and the formation of secondary amines.[26] The second stage occurs between 344 and 416 °C, with a mass loss of approximately 54.18%. This stage mainly involves the decomposition of soft segments, involving the decomposition of residual fragments produced by the degradation in the first stage.[27] The final solid residue is 15.53%. Pre-PUF and PUF-HS exhibit thermal degradation 28 °C earlier in the first stage, as the roughing process disrupts the chemical structure of the PUF molecular chains. The primary mass loss range for PUF-HS is 320–402 °C, with a mass loss of approximately 46.21%, and the final solid residue is 17.45%. Compared to PUF and pre-PUF, PUF-HS have a higher residual content, possibly due to the formation of SiO_2 during thermal decomposition.[28] As shown in Fig. 6b, the weight loss peaks of pre-PUF and PUF-HS are significantly shifted to lower temperatures, which can be attributed to the strong oxidizing properties of the roughening solution. This solution damages the molecular structure of PUF, leading to premature thermal degradation.

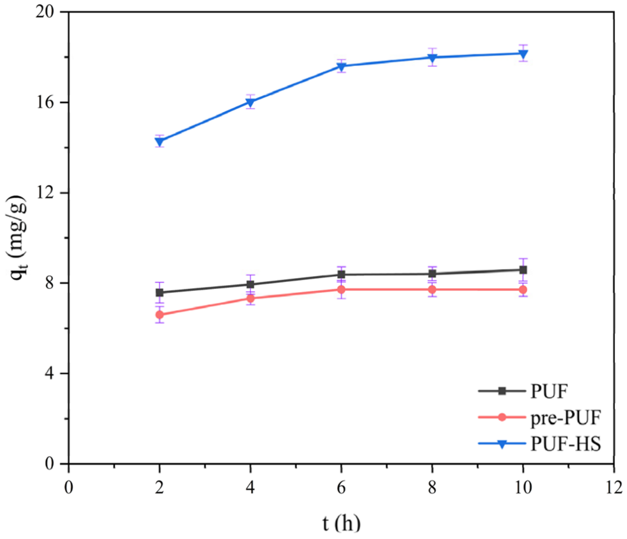

Fig. 7 Adsorption capacity of PUF, pre-PUF and PUF-HS on Hg(II).

3.2 Static adsorption

The adsorption capacities of PUF, pre-PUF, and PUF-HS for Hg(II) were investigated, as shown in Fig. 7. At an adsorption time of 10 h, the adsorption capacities of PUF, pre-PUF, and PUF-HS for Hg(II) are 8.65, 7.78, and 18.17 mg g^{-1}, respectively. Notably, the adsorption capacity of PUF-HS for Hg(II) is significantly higher than that of PUF and pre-PUF, which can be attributed to the excellent binding ability of the thiol functional groups in PUF-HS toward Hg(II).[29]

3.3 Effect of solution pH

Adsorption experiments were conducted within the pH range of 1.0 to 6.0 to investigate the effect of solution pH on the adsorption performance of PUF-HS toward Hg(II). As shown in

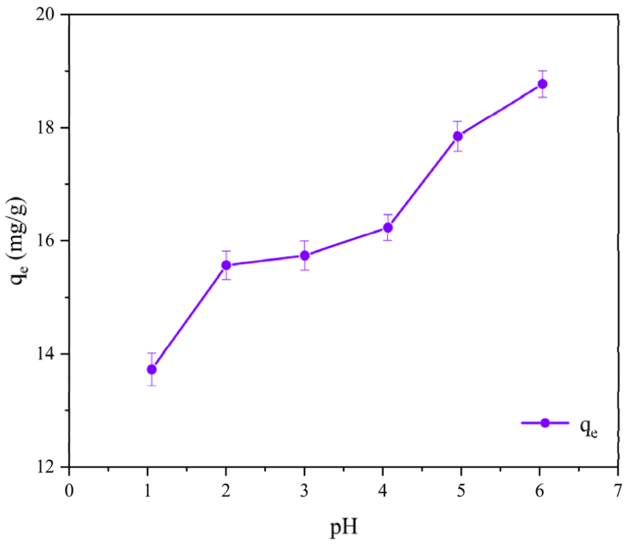

Fig. 8 Effect of solution pH on the adsorption performance of Hg(II) by PUF-HS.

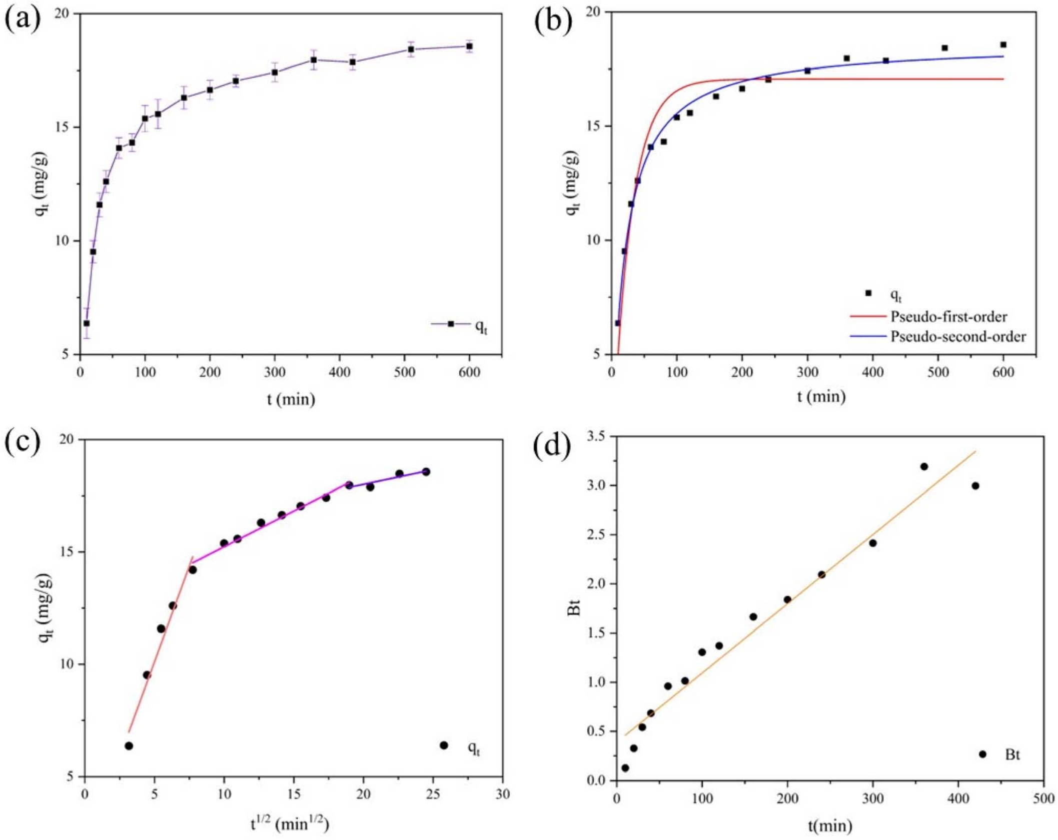

Fig. 9 Kinetic fitting curves of Hg(II) adsorption by PUF-HS: (a) effect of contact time on adsorption capacity, (b) pseudo-first-order and pseudo-second-order models, (c) intra-particle diffusion model, (d) Boyd model.

Fig. 8, the adsorption capacity of PUF-HS increases with increasing pH, from 13.71 mg g^{-1} to 18.75 mg g^{-1}. At pH < 4.0, the adsorption efficiency is poor because the high H^+ concentration in acidic conditions causes protonation of the adsorption sites on PUF-HS, thereby reducing the adsorption capacity. When the solution pH > 4.0, the H^+ concentration gradually decreases, and the active sites undergo deprotonation, making them more accessible for binding with metal ions. The optimal adsorption efficiency is achieved at pH = 6.0.

3.4 Adsorption kinetics

Kinetic experiments were conducted at different adsorption times. The adsorption experimental data were fitted using the pseudo-first-order model, pseudo-second-order model, intra-particle diffusion model, and Boyd model to study the equilibrium time, equilibrium adsorption amount, and kinetic mechanism of the adsorption process. As shown in Fig. 9a, PUF-HS rapidly adsorbs within 80 min, with the adsorption amount increasing to 14.32 mg g^{-1}. During this stage, Hg(II) comes into contact with active sites on the surface of PUF-HS, such as –SH, –NH–, and –OH. After 80 min, as the internal active sites of PUF-HS are gradually occupied, the adsorption rate decreases, and the process approaches saturation. After 510 min, the equilibrium adsorption capacity reaches 18.42 mg g^{-1}. The fitting results and relevant parameters of adsorption kinetics are presented in Fig. 9b and Table 1. Based on the kinetic model fitting data, the correlation coefficient ($R^2 = 0.9916$) for the pseudo-second-order model is higher than that for the pseudo-first-order model ($R^2 = 0.9121$), indicating that the kinetic data for PUF-HS adsorption fits better with the pseudo-second-order

Table 1 Fitting parameters of pseudo-first-order, pseudo-second-order, intra-particle diffusion, and Boyd models for Hg(II) adsorption onto PUF-HS

Pseudo-first-order		Pseudo-second-order		Intra-particle diffusion			Boyd
$q_{e,\text{ cal}}$, mg g^{-1}	k_1 min^{-1} (R^2)	$q_{e,\text{ cal}}$, mg g^{-1}	k_2 g $(\text{mg min})^{-1}$ (R^2)	k_{ip1} mg $(\text{g min}^{1/2})^{-1}$ (R^2)	k_{ip2} mg $(\text{g min}^{1/2})^{-1}$ (R^2)	k_{ip3} mg $(\text{g min}^{1/2})^{-1}$ (R^2)	k_d mg $(\text{g min})^{-1}$ (R^2)
17.06	0.03502 (0.9121)	18.64	0.00271 (0.9916)	1.702 (0.9643)	0.3175 (0.9788)	0.1304 (0.8379)	0.00704 (0.9601)

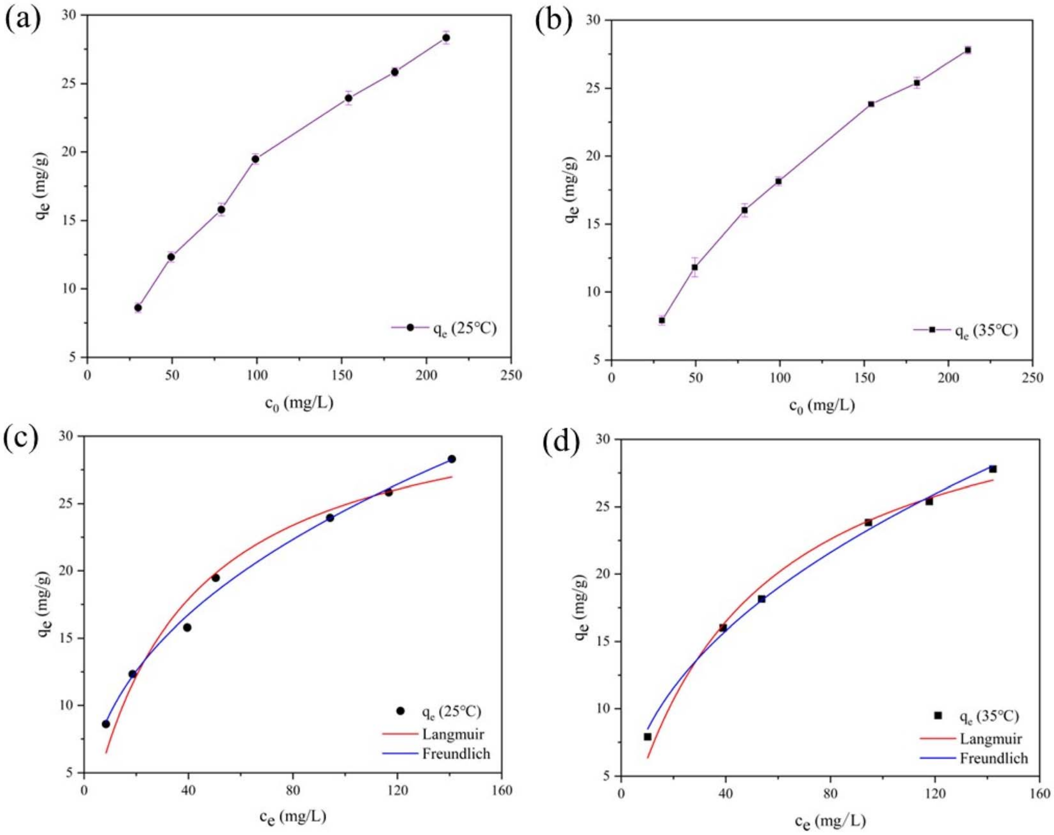

Fig. 10 Effect of initial concentration on the adsorption of Hg(II) by PUF-HS at different temperatures: (a) 25 °C and (b) 35 °C, Langmuir and Freundlich isothermal adsorption curves at different temperatures: (c) 25 °C and (d) 35 °C.

model. This further confirms that the Hg(II) adsorption process is dominated by chemisorption,[30,31] which suggests interactions (*e.g.*, ion exchange and chelation) occur between PUF-HS and Hg(II).[32] To further explore the role of Hg(II) diffusion in the adsorption process, kinetic analysis was performed *via* the Weber–Morris intra-particle diffusion model. Fig. 9c shows the fitting curve of the intra-particle diffusion model, which exhibits a three-segment linear profile with a gradual decrease in the intraparticle diffusion rate constant (k_{ip}) over time. This indicates that the overall adsorption process is relatively complex and regulated by multiple factors.[33] The adsorption process of PUF-HS for Hg(II) can thus be divided into three distinct stages. The first stage is mainly surface diffusion, during which Hg(II) diffuses from the solution to the surface of the adsorbent. The second stage is mainly internal diffusion, where Hg(II) migrates through the interior of the particles to the inner surface of the adsorbent's pores.[34] The final stage is the equilibrium stage, indicating that the adsorption sites of the adsorbent are completely occupied by Hg(II). The linear segment of the second stage does not pass through the origin, suggesting that intraparticle diffusion is not the only rate-limiting step.[35] Further analysis using the Boyd model confirmed that film diffusion is an additional rate-limiting step, as shown in Fig. 9d. In this plot, *Bt* exhibits a linear relationship with time (*t*) and does not pass through the origin.[35] By comparing the correlation coefficients (R^2) derived from fitting different kinetic models, the pseudo-second-order kinetic model was found to be the most suitable for describing the adsorption process. This indicates that chemisorption is the dominant factor governing the adsorption behavior of PUF-HS for Hg(II).[36] In summary, the adsorption process is influenced by chemisorption between Hg(II) and the active sites of PUF-HS, as well as by intraparticle diffusion and film diffusion.[37]

3.5 Adsorption isotherms

To investigate the effect of initial Hg(II) concentration on the adsorption performance of PUF-HS, a series of adsorption experiments were conducted using Hg(II) solutions with varying initial concentrations, as shown in Fig. 10a and b. With the increase in initial concentration, the adsorption capacity of PUF-HS for Hg(II) first increases rapidly and then gradually approaches equilibrium. At 25 °C, when the initial concentration of the Hg(II)

Table 2 Adsorption isotherm model fitting parameters for Hg(II) adsorption onto PUF-HS

	Langmuir			Freundlich		
T (°C)	q_m (mg g^{-1})	K_L (L mg^{-1})	$R_L{}^2$	K_F (kJ mol^{-1})	n	$R_F{}^2$
25	33.74	0.02826	0.9643	3.6234	2.409	0.9938
35	35.96	0.02111	0.9804	2.9761	2.211	0.9957

Table 3 Some thiol-functionalized polymer/foam adsorbents

Adsorbents	Metal ion	q_m (mg g^{-1})	Optimal adsorption kinetic model	Selective	Ref.
CHAP-SH	Hg(II)	282.74 (pH = 4.5, c_0 = 50–300 mg L^{-1})	Pseudo-second-order (R^2 = 0.9614)	Hg(II)	40
PAM-SH	Hg(II)	82 (c_0 = 50–250 mg L^{-1})	Pseudo-second-order (R^2 = 0.9632)	Hg(II)	41
Chi-SH	As(III)	21.01 (pH = 7, c_0 = 5–15 mg L^{-1})	Pseudo-second-order (R^2 = 0.994)	As(III)	42
Au-AG	Hg(II)	12.82 (c_0 = 17.6–176 μg L^{-1})	Pseudo-second-order (R^2 = 0.994)	—	43
DE/Pb(II)IIP	Pb(II)	79.38	Pseudo-second-order (R^2 = 0.9998)	Pb(II)	44
PAA-*g*-PUf	Pb(II)	256.4 (pH = 6, c_0 = 0–500 mg L^{-1})	Pseudo-second-order (R^2 = 0.986)	—	8
SG-ODPPNE	Hg(II)	13.5 (pH = 8, c_0 = 1–100 mg L^{-1})	Pseudo-second-order (R^2 = 0.9953)	Hg(II)	45
TC nanofiber	Pb(II)	22 (pH = 4, c_0 = 20–400 mg L^{-1})	Pseudo-second-order (R^2 = 0.999)	—	46
PU@PZDS	Pb(II)	228.3 (c_0 = 10–500 mg L^{-1})	Pseudo-first-order (R^2 = 0.989)	—	20
Sil-PU	Cu(II)	46.13 (pH = 3.5, c_0 = 20–200 mg L^{-1})	Pseudo-second-order (R^2 = 0.982)	—	47
This work	Hg(II)	35.96 (pH = 6.0, c_0 = 29.9–211.6 mg L^{-1})	Pseudo-second-order (R^2 = 0.9916PUF)	Hg(II)	
PVAm-MMB	Hg(II)	62.9 (pH = 4.5, c_0 = 10–500 mg L^{-1})	Pseudo-second-order (R^2 = 0.9958)	Cd(II)	48

solution rises from 29.9 mg L^{-1} to 211.6 mg L^{-1}, the adsorption capacity of PUF-HS increases from 8.61 mg g^{-1} to 28.30 mg g^{-1}. This phenomenon is attributed to the enhanced mass transfer driving force of Hg(II) from the aqueous phase to the solid phase at higher concentrations,[38] leading to a gradual increase in the adsorption capacity of PUF-HS.

The Langmuir and Freundlich isotherm models were employed to fit the experimental data and explore the adsorption mechanism of PUF-HS for Hg(II). Fig. 10c and d display the fitted curves of the Langmuir and Freundlich isotherm models at 25 °C and 35 °C, respectively. Table 2 summarizes the relevant parameters derived from the isotherm model fitting. The fitting results reveal that temperature variations have a negligible effect on adsorption efficiency. At 25 °C, the correlation coefficients (R^2) of the Langmuir and Freundlich isotherm models are 0.9643 and 0.9938, respectively. Notably, the Freundlich isotherm model exhibits superior fitting performance, suggesting that the adsorption process involves multilayer adsorption.[39] According to the fitting data of the Langmuir isotherm model, the maximum adsorption capacities of PUF-HS for Hg(II) at 25 °C and 35 °C are 33.74 mg g^{-1} and 35.96 mg g^{-1}, respectively.

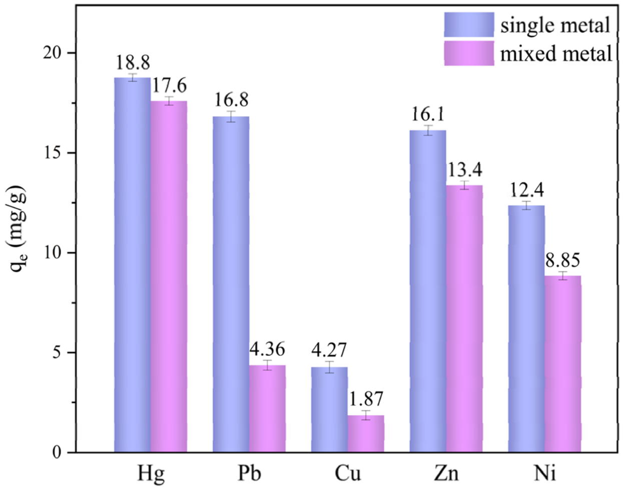

Fig. 11 Effect of co-existing metal ions on the adsorption of Hg(II) by PUF-HS: single metal ion and mixed metal ion solutions.

Table 3 summarizes representative thiol-functionalized polymer/foam adsorbents reported in recent years. Compared with other adsorbents, PUF-HS exhibits a moderate Hg(II) adsorption capacity. Although its adsorption capacity is lower than that of the previously reported CHAP-SH and PVAm-MMB, PUF-HS eliminates the need for high-temperature activation, the preparation process is simple, and provides a novel strategy for the utilization of waste polyurethane foam.

3.6 Selective adsorption

Selective adsorption experiments of PUF-HS toward Hg(II) were conducted in 20 mL solutions containing single and mixed metal ions (Hg(II), Pb(II), Cu(II), Zn(II), and Ni(II)), aiming to investigate the interference of coexisting metal ions on Hg(II) adsorption. The adsorption capacities of different metal ions in single and mixed solutions are shown in Fig. 11. In single metal solutions, PUF-HS exhibits an adsorption capacity of 18.8 mg g^{-1} for Hg(II), compared to 16.8 mg g^{-1} for Pb(II), 4.27 mg g^{-1} for Cu(II), 16.1 mg g^{-1} for Zn(II), and 12.4 mg g^{-1} for Ni(II). In mixed metal solutions, the adsorption capacities for Hg(II), Pb(II), Cu(II), Zn(II), and Ni(II) are 17.6 mg g^{-1}, 4.36 mg g^{-1}, 1.87 mg g^{-1}, 13.4 mg g^{-1}, and 8.85 mg g^{-1}, respectively. Notably, PUF-HS shows significantly higher adsorption capacity for Hg(II) than other heavy metal ions in both solution systems, demonstrating its excellent adsorption selectivity toward Hg(II).

3.7 Effect of ionic strength on Hg(II) adsorption

To evaluate the effect of ionic strength on Hg(II) adsorption by PUF-HS, NaCl was added to the Hg(II) solution as the background electrolyte. As shown in Fig. 12a, at 25 °C, the maximum Hg(II) adsorption capacity of PUF-HS decreased from 25.82 mg g^{-1} to 18.18 mg g^{-1} as the NaCl concentration increased from 0.01 mol L^{-1} to 0.1 mol L^{-1}. Compared with the Hg(II) solution without NaCl, the maximum adsorption capacity of PUF-HS in the 0.01 mol L^{-1} NaCl-containing Hg(II) solution decreased by 8%. These results indicate that NaCl inhibits Hg(II) adsorption by PUF-HS, with the inhibitory effect becoming more pronounced as ionic strength increases. The underlying mechanism is associated with the strong complexation between Cl$^-$ and Hg(II). At low ionic strengths, Hg(II) primarily exists in

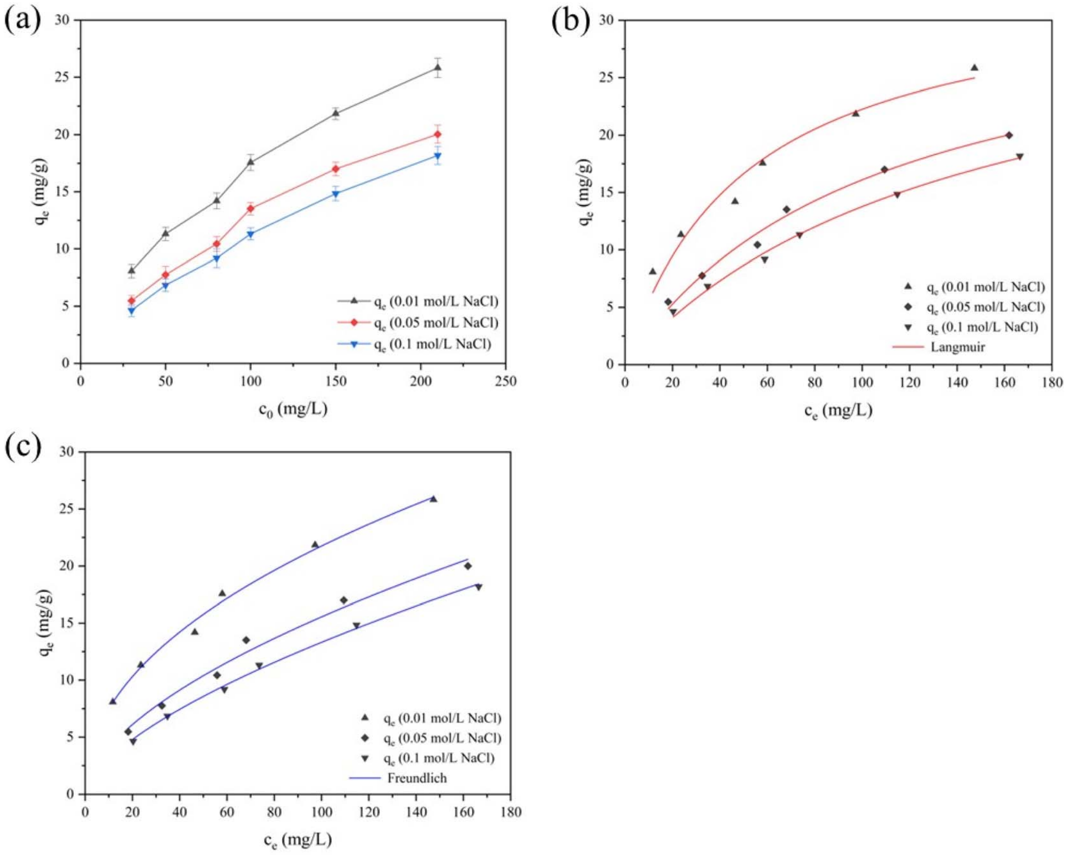

Fig. 12 Effect of ionic strength on Hg(II) adsorption by PUF-HS at 25 °C (a) adsorption isotherm models at different ionic strengths: (b) Langmuir and (c) Freundlich.

Table 4 Adsorption isotherm model fitting parameters for Hg(II) adsorption onto PUF-HS at different ionic strengths

	Langmuir			Freundlich		
Ionic strengths	q_m (mg g^{-1})	K_L (L mg^{-1})	$R_L{}^2$	K_F (kJ mol^{-1})	n	$R_F{}^2$
0.01 mol L^{-1} NaCl	33.61	0.01962	0.9640	2.570	2.157	0.9921
0.05 mol L^{-1} NaCl	33.08	0.00948	0.9861	1.068	1.720	0.9840
0.1 mol L^{-1} NaCl	33.54	0.00693	0.9934	0.7127	1.573	0.9967

solution as the uncharged species HgClOH and $HgCl_2$. In contrast, at higher ionic strengths (*i.e.*, with increased Cl^- concentration), Hg(II) is predominantly present as the negatively charged species $HgCl_4{}^{2-}$ and $HgCl_3{}^-$.[49,50] Fig. 12b and c display the fitted curves of the Langmuir and Freundlich isotherm models, respectively, obtained from adsorption experiments at different NaCl concentrations. The results show that the Freundlich isotherm model provides a better fit, indicating that the adsorption process follows a multi-layer mechanism.[39] The relevant parameters obtained by fitting the isotherm model are shown in Table 4.

3.8 Influence of natural organic matter on Hg(II) adsorption

Humic acid (HA), a naturally occurring organic substance, is ubiquitous in aquatic environments. Its structure contains abundant organic functional groups that can form stable chelates with various heavy metals, thereby affecting the Hg(II) removal efficiency of PUF-HS.[51] Fig. 13a shows that at 25 °C, the actual Hg(II) adsorption capacity of PUF-HS reached a maximum of 32.96 mg g^{-1} when the HA concentration was 20 mg L^{-1}. With a further increase in HA concentration, the Hg(II) adsorption capacity of PUF-HS decreased slightly. Notably, compared with the HA-free Hg(II) solution, the maximum Hg(II) adsorption capacity of PUF-HS in the 20 mg L^{-1} HA-containing Hg(II) solution increased by 17%, indicating that HA can promote the adsorption of Hg(II). Fig. 13b and c display the fitted curves of the Langmuir and Freundlich isotherm models, respectively, derived from adsorption experiments at different HA concentrations. Table 5 summarizes the relevant parameters obtained from the isotherm model fitting. The results show that the Langmuir isotherm model provided a better fit to the data, indicating a monolayer adsorption mechanism.[52] This

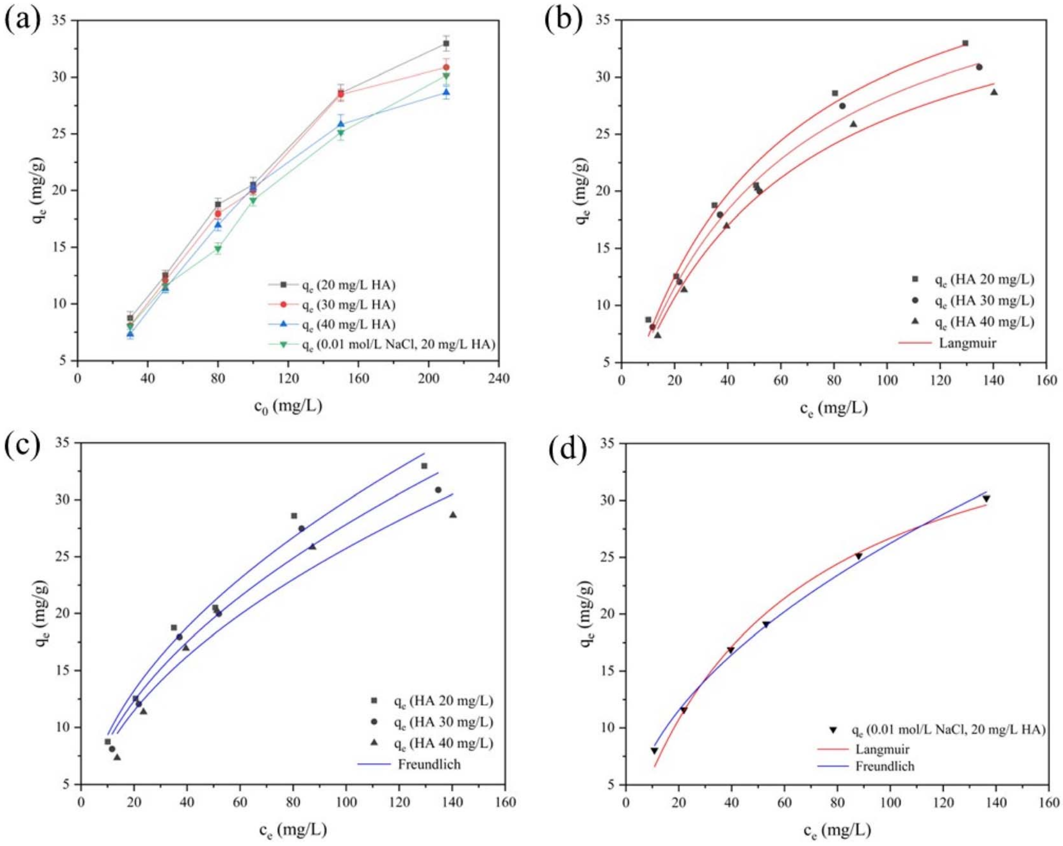

Fig. 13 (a) Effect of humic acid on Hg(II) adsorption by PUF-HS at 25 °C, (b) Langmuir for different humic acid concentrations, (c) Freundlich for different humic acid concentrations, and (d) Langmuir and Freundlich for 0.01 mol L^{-1} NaCl and 20 mg L^{-1} HA concentration.

Table 5 Adsorption isotherm model fitting parameters for Hg(II) adsorption onto PUF-HS at different humic acid concentrations

	Langmuir			Freundlich		
Humic acid concentrations	q_m (mg g^{-1})	K_L (L mg^{-1})	R_L^2	K_F (kJ mol^{-1})	n	R_F^2
20 mg L^{-1} HA	46.62	0.01836	0.9838	2.906	1.976	0.9821
30 mg L^{-1} HA	44.26	0.01771	0.9911	2.708	1.977	0.9730
40 mg L^{-1} HA	41.54	0.01732	0.9823	2.685	1.991	0.9510
0.01 mol L^{-1} NaCl, 20 mg L^{-1} HA	42.42	0.01696	0.9920	2.505	1.961	0.9963

may be attributed to the fact that upon entering the adsorption system, HA forms a uniform coating on the surface of PUF-HS *via* specific interaction pathways, which in turn modifies the interfacial properties of the adsorbent.[53,54] This modification shifts the adsorption behavior from a "Freundlich-type" to a "Langmuir-type" process.

Isothermal adsorption experiments were performed at 25 °C under controlled conditions, including 0.01 mol L^{-1} NaCl and 20 mg L^{-1} HA concentration. As shown in Fig. 13a, PUF-HS retained a high Hg(II) adsorption capacity, indicating that the enhancing effect of HA is dominant. As illustrated in Fig. 13d and Table 5, both isotherm models exhibited excellent fitting performance with the experimental data; thus, no further comparison between them was conducted. Fitting of the experimental data to the Langmuir isotherm model revealed that the maximum Hg(II) adsorption capacity of PUF-HS is 42.42 mg g^{-1}.

4 Adsorption mechanism

To investigate the adsorption mechanism of Hg(II) by PUF-HS, FTIR and XPS analyses were performed on the material before and after adsorption. FTIR was used to analyze the changes in surface functional groups of PUF-HS before and after Hg(II) adsorption, as shown in Fig. 14. After adsorbing Hg(II), the stretching vibration peak of the N–H groups shifts from 3290 cm^{-1} to 3285 cm^{-1}, which may be attributed to the interaction between the N–H groups and Hg(II). In the wavenumber ranges of 1220–1140 cm^{-1} and 720–610 cm^{-1} regions, the peak shapes of the C–S groups in PUF-HS after Hg(II)

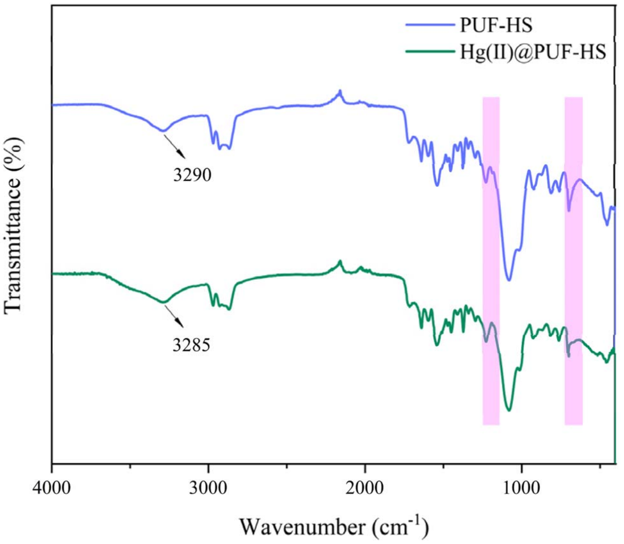

Fig. 14 FTIR analysis of PUF-HS and Hg(II)@PUF-HS.

adsorption both changed. This observation is likely due to the formation of complexes between –SH groups and Hg(II) ions.

XPS analysis was conducted to investigate the chemical states of elements in PUF-HS after Hg(II) adsorption, as shown in Fig. 15. From the XPS full spectra of PUF-HS and Hg(II)@PUF-HS (Fig. 15a), the characteristic peak of Hg 4f is detected after Hg(II) adsorption, confirming successful Hg(II) uptake and the N 1s characteristic peak shifts from 399.5 eV to 399.9 eV, which attribute to the chelation of N–H groups with Hg(II). As shown in Fig. 15b, after Hg(II) adsorption, the peaks of $2p_{3/2}$ and $2p_{1/2}$ in the S 2p spectrum shift from 163.3 eV and 164.5 eV to 163.79 eV and 164.98 eV, respectively, indicating a shift of S 2p peaks toward higher binding energies. This reflects an increase in the oxidation state of sulfur,[48] suggesting that the –SH groups have undergone chelation reactions with Hg(II). Additionally, the Hg 4f spectrum of PUF-HS after Hg(II) adsorption (Fig. 15c) deconvolves into two independent peaks corresponding to the $4f_{5/2}$ and $4f_{7/2}$ spin–orbit split energy levels, with binding energies of 105.67 eV and 101.72 eV, respectively, and a spin–orbit splitting of 3.95 eV. This indicates that Hg(II) is adsorbed in the oxidation state (+II).[55] As shown in Table 6, the atomic percentage of Hg(II) is 1.48%. These results indicate that the adsorption of Hg(II) by PUF-HS is primarily driven by chelation interactions between –SH/–NH groups and Hg(II).

Table 6 Hg(II)@PUF-HS elemental percentages from XPS full spectrum

Name	Peak BE	FWHM (eV)	Atomic (%)
C 1s	285.81	3.05	36.87
N 1s	399.93	1.63	3.06
O 1s	532.53	1.98	17.42
Si 2p	101.08	2.14	34.6
S 2p	163.17	1.43	3.35
Cl 2p	198.88	3.71	3.21
Hg 4f	101.08	1.99	1.48

5. Conclusion

This study presents a simple two-step method for converting waste PUF into thiol-functionalized adsorbent (PUF-HS). SEM images of PUF-HS reveal that it retains a highly porous three-dimensional network structure, while its surface becomes rougher with numerous protruding particles. When combined with BET analysis results, it is confirmed that PUF-HS contains only micropores and macropores. The FTIR spectrum of PUF-HS shows stretching vibration peaks of Si–O–Si and C–S groups, and new characteristic peaks of S 2p and Si 2p appear in the XPS full spectrum, confirming the successful grafting of –SH groups onto the PUF surface. In the TG curve, the residual mass of PUF-HS is higher than that of PUF and pre-PUF, attributed to the decomposition of condensed silanes during thermal degradation, leading to the formation of SiO_2. Adsorption experiments demonstrate that PUF-HS efficiently removes Hg(II) from aqueous solutions. Kinetic and isothermal analyses reveal that this adsorption behavior fits well with the pseudo-second-order kinetic model and the Freundlich isotherm model, respectively. The adsorption was multilayer adsorption dominated by chemical adsorption and controlled by intra-particle diffusion and film diffusion. Notably, PUF-HS retains high Hg(II) adsorption capacity even in mixed metal ion solutions, demonstrating excellent adsorption selectivity for Hg(II).

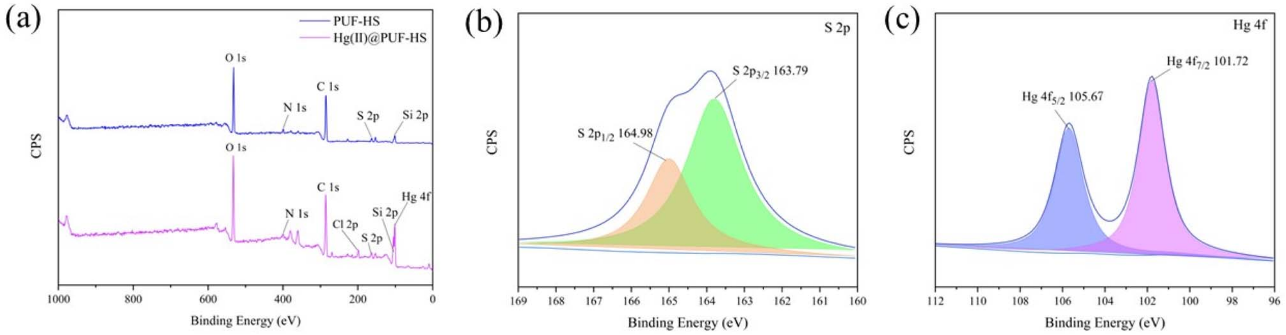

Fig. 15 (a) XPS full spectra of PUF-HS and Hg(II)@PUF-HS; (b) high-resolution S 2p spectra of Hg(II)@PUF-HS; (c) high-resolution Hg 4f spectra of Hg(II)@PUF-HS.

Additionally, under controlled ionic strength (0.01 mol L^{-1} NaCl), adsorption experiments involving natural organic matter (*i.e.*, humic acid) show that PUF-HS maintains favourable Hg(II) adsorption capacity which indicating strong environmental adaptability for Hg(II) removal. FTIR and XPS analyses of PUF-HS before and after adsorption reveal that the adsorption of Hg(II) is primarily driven by chelation between –SH/–NH groups and Hg(II). This work may have promising application potential in Hg(II)-containing wastewater treatment and regional water environment protection.

Author contributions

Meixin Chen: investigation, formal analysis, writing – original draft, writing – review & editing; Lili Zhu: methodology, writing – review & editing; Juan Jin: supervision, visualization, writing – review & editing; Cunxin Sun: visualization, writing – review & editing; Zhenjiang Zhang: formal analysis, supervision, visualization, writing – review & editing.

Conflicts of interest

There are no conflicts of interest to declare.

Data availability

The data supporting this article have been included as part of the supplementary information (SI). Supplementary information: the BET analysis of PUF-HS. See DOI: https://doi.org/10.1039/d5ra05379j.

Acknowledgements

This research was supported by the Shandong Province Science and Technology-based Small and Medium-sized Enterprise Innovation Capacity Enhancement Project (No. 2022TSGC2307 and 2023TSGC0844) and the Natural Science Foundation of Shandong Province (No. ZR2024ME213, ZR2017PB006), the Open Foundation of State Key Laboratory of Inorganic Synthesis and Preparative Chemistry of Jilin University (No. 2023-20), the Teaching Reform Research Project of Undergraduate Universities in Shandong Province (No. M2022181).

References

1 A. Pratush, A. Kumar and Z. Hu, *Int. Microbiol.*, 2018, **21**, 97–106.
2 C. Zamora-Ledezma, D. Negrete-Bolagay, F. Figueroa, E. Zamora-Ledezma, M. Ni, F. Alexis and V. H. Guerrero, *Environ. Technol. Innov.*, 2021, **22**, 101504.
3 E. O. Alegbe and T. O. Uthman, *Heliyon*, 2024, **10**, e33646.
4 X. F. Hu, M. Lowe and H. M. Chan, *Environ. Res.*, 2021, **193**, 110538.
5 A. E. Charkiewicz, W. J. Omeljaniuk, M. Garley and J. Nikliński, *Int. J. Mol. Sci.*, 2025, **26**, 2326.
6 A. Amin, M. Saadatakhtar, A. Mohajerian, S. M. Marashi, S. Zamanifard, A. Keshavarzian, P. Molaee, M. S. Keshmiri and F. Nikdoust, *Cardiovasc. Toxicol.*, 2025, **25**, 507–522.
7 A. S. Ramamurthy and R. Memarian, *Water, Air, Soil Pollut.*, 2012, **223**, 511–518.
8 K. K. Singh, N. K. Goel, A. Kanjilal, R. Ruhela, V. Kumar, K. Bhattacharyya and A. K. Tyagi, *Polym. Bull.*, 2024, **81**, 13435–13460.
9 M. G. Motitswe, K. O. Badmus and L. Khotseng, *Catalysts*, 2022, **12**, 1057.
10 R. Selvasembian, W. Gwenzi, N. Chaukura and S. Mthembu, *J. Hazard. Mater.*, 2021, **417**, 125960.
11 S. Wu, S. P. Ma, Q. H. Zhang and C. Yang, *Polymer*, 2025, **327**, 128361.
12 G. A. Meligi, *Polym.-Plast. Technol. Eng.*, 2007, **47**, 106–113.
13 M. Lakshmipathy, M. Chandrasekaran and R. Kulanthasamy, *Acta Chim. Slov.*, 2020, **67**, 602–608.
14 L. F. Ren, Z. Tang, J. Y. Du, L. Chen and T. T. Qiang, *J. Hazard. Mater.*, 2021, **417**, 126130.
15 X. Y. Zhang, Z. Li, K. S. Liu and L. Jiang, *Adv. Funct. Mater.*, 2013, **23**, 2881–2886.
16 X. H. Wang, R. Z. Sun and C. Y. Wang, *Colloid Surf. A*, 2014, **441**, 51–58.
17 H. Wang, G. H. Ma, K. Zhang, Z. Jia, Y. Z. Wang, L. Gao and B. X. Liu, *Materials*, 2023, **16**, 4583.
18 D. Quang Khieu, B. H. Dang Son, V. Thi Thanh Chau, P. Dinh Du, N. Hai Phong and N. Thi Diem Chau, *J. Chem.*, 2017, 1–10, DOI: 10.1155/2017/9560293.
19 G. Mondin, M. R. Lohe, F. M. Wisser, J. Grothe, N. Mohamed-Noriega, A. Leifert, S. Dörfler, A. Bachmatiuk, M. H. Rümmeli and S. Kaskel, *Electrochim. Acta*, 2013, **114**, 521–526.
20 Y. L. Huang, L. L. Liu, C. Y. Hu, Y. Li, H. P. He, Z. Y. Chen and Y. W. Huang, *ACS Appl. Polym. Mater.*, 2022, **4**, 7373–7386.
21 F. Ke, J. Jiang, Y. Z. Li, J. Liang, X. C. Wan and S. Ko, *Appl. Surf. Sci.*, 2017, **413**, 266–274.
22 S. Xiong, Z. X. Zhong and Y. Wang, *AIChE J.*, 2017, **63**, 2232–2240.
23 C. M. Carr, I. H. Leaver and A. E. Hughes, *Text. Res. J.*, 1986, **56**, 216–217.
24 X. Li, Y. X. Ma, X. F. Shi, X. Y. Kang, F. M. Bai and D. J. Zhang, *Desalin. Water Treat.*, 2021, **226**, 419–430.
25 M. Strankowski, P. Korzeniewski, J. Strankowska, A. A. S and S. Thomas, *Materials*, 2018, **11**, 82.
26 I. Javni, Z. S. Petrovi, A. Guo and R. Fuller, *J. Appl. Polym. Sci.*, 2000, **77**, 1723–1734.
27 Ł. Piszczyk, P. Kosmela and M. Strankowski, *Adv. Polym. Technol.*, 2017, **37**, 1625–1634.
28 D. M. Nanicuacua, M. G. Segatelli, M. Z. Corazza and C. R. Teixeira Tarley, *Anal. Methods*, 2016, **8**, 2820–2830.
29 X. C. Wang, Z. M. Dai, X. Zhou, H. Chen, Y. Cao, J. H. Hou and X. Z. Wang, *Prog. Nat. Sci.: Mater. Int.*, 2023, **33**, 644–651.
30 S. Soleimani, A. Heydari, M. Fattahi and A. Motamedisade, *Ind. Crops Prod.*, 2023, **192**, 115999.
31 J. Q. Zhang, Z. Wang, Y. Luo, Z. L. Zhang, X. Y. Feng, Q. Zeng, D. Tian, C. Li, Y. D. Zhang and S. Chen, *Minerals*, 2023, **13**, 1337.

32 K. Wang, Z. Song, Z. Xu, Y. Xi, Y. Cui and H. Zhou, *RSC Adv.*, 2025, **15**, 21121–21132.

33 H. Zeng, F. Wang, K. Xu, J. Zhang and D. Li, *Int. J. Biol. Macromol.*, 2020, **149**, 1222–1231.

34 S. F. Sun, H. F. Wan, X. Zhao, C. Gao, L. P. Xiao and R. C. Sun, *Int. J. Biol. Macromol.*, 2023, **253**, 126688.

35 S. Dubey, R. K. Mishra, S. Kaya, E. R. Rene, B. S. Giri and Y. C. Sharma, *Chemosphere*, 2024, **355**, 141696.

36 Q. Zhang, Y. Zhao, L. Qin, W. Liang, K. Chen, K. Li and R. Yan, *J. Radioanal. Nucl. Chem.*, 2024, **333**, 5347–5361.

37 E. Cheraghipour and M. Pakshir, *Chemosphere*, 2020, **260**, 127560.

38 H. J. Dai, Y. Huang, H. Zhang, L. Ma, H. H. Huang, J. H. Wu and Y. H. Zhang, *Carbohydr. Polym.*, 2020, **230**, 115599.

39 Y. L. Bai, H. Ge, Q. Li, F. Xie and W. Wang, *Materials*, 2025, **18**, 1526.

40 Q. Wang, S. Zhu, C. Xi, B. Jiang and F. Zhang, *ACS Omega*, 2022, **7**, 12231–12241.

41 M. Zhu, X. Wang, Y. Huang, L. Yue, S. Zhong and L. Zeng, *J. Appl. Polym. Sci.*, 2022, **139**, e52976.

42 Y. Ye, T. Zhang, L. Lv, Y. Chen, W. Tang and S. Tang, *Colloid Surf. A*, 2021, **622**, 126601.

43 S. K. Sharma, E. Yosef, H. Mamane and R. Kumar, *RSC Adv.*, 2025, **15**, 23910–23919.

44 X. Li, W. Xu, Y. Yang, B. Li, G. Pan, N. Chen and Q. Xie, *Mater. Today Commun.*, 2023, **36**, 106434.

45 S. W. Khor, Y. K. Lee, M. R. B. Abas and K. S. Tay, *J. Sol-Gel Sci. Technol.*, 2017, **82**, 834–845.

46 H. Y. Choi, J. H. Bae, Y. Hasegawa, S. An, I. S. Kim, H. Lee and M. Kim, *Carbohydr. Polym.*, 2020, **234**, 115881.

47 B. Merillas, M. Á. Rodríguez-Pérez and L. Durães, *J. Ind. Eng. Chem.*, 2025, **146**, 578–588.

48 N. Zouli, N. Maslamani, M. Hassan, M. F. Cheira and T. F. Hassanein, *J. Ind. Eng. Chem.*, 2025, **149**, 836–848.

49 K. Gai, A. Avellan, T. P. Hoelen, F. Lopez-Linares, E. S. Hatakeyama and G. V. Lowry, *Water Res.*, 2019, **157**, 600–609.

50 J. Wang, B. L. Deng, H. Chen, X. R. Wang and J. Z. Zheng, *Environ. Sci. Technol.*, 2009, **43**, 5223–5228.

51 P. Pei, Y. Xu, L. Wang, X. Liang and Y. Sun, *Sci. Total Environ.*, 2022, **806**, 150510.

52 Y. Wang, H. Liu, W. Wang, B. Yin, H. Wang, F. Zhang, J. Wang and Z. Huang, *Environ. Pollut.*, 2025, **367**, 125657.

53 L. Xie, Q. Lu, X. Mao, J. Wang, L. Han, J. Hu, Q. Lu, Y. Wang and H. Zeng, *Water Res.*, 2020, **176**, 115766.

54 G. Jin, Y. Eom and T. G. Lee, *J. Ind. Eng. Chem.*, 2016, **42**, 46–52.

55 L. Zhao, Y. Zhang, L. Wang, H. Lyu, S. Xia and J. Tang, *Chemosphere*, 2022, **294**, 133820.